Drying-Induced Consolidation in Soil

Yi Dong, M.ASCE[1]; Ning Lu, F.ASCE[2]; and Patrick J. Fox, F.ASCE[3]

Abstract: Drying-induced consolidation in soil is defined as volumetric shrinkage by interparticle stresses (suction stress) during drying under conditions of zero external or total stress. A new analysis is presented to synthesize recently published and new experimental data for soil water retention, shrinkage, physicochemical properties, and index properties for a broad range of soils ranging from nonexpansive to highly expansive. The suction stress characteristic curves of these soils are computed and compared using two deformation-based methods: the previously established discretized element solution and a simpler bulk-volume solution. Drying-induced consolidation for unsaturated soils exhibits a similar behavior to traditional consolidation behavior for saturated soils. The demonstrated strong correlations between the compression index and soil water retention characteristics and between the compression index and geotechnical index properties provide rational linkages between the fundamental soil properties and bulk deformation properties, where in this case the compression index is defined as the slope of the void ratio versus logarithm of negative suction stress relationship. These correlations are expected to be useful as new fundamental index properties for soil classification and for geotechnical applications involving desiccation and volume change.
DOI: 10.1061/(ASCE)GT.1943-5606.0002327.

Author keywords: Consolidation; Soil shrinkage; Soil water retention curve; Suction stress; Unsaturated soil; Specific surface area; Cation-exchange capacity; Atterberg limits.

Introduction

Consolidation is a fundamental process of soil mechanics and was described by Terzaghi (1943) as "a decrease of water content of a saturated soil without replacement of the water by air." Most commonly, consolidation occurs when soil is subjected to an increase in applied stress. At the first instant of loading for saturated soils, the applied stress is carried almost entirely by the pore water due to the contrast between the essentially incompressible liquid phase and the more compressible soil skeleton. In time, drainage of pore water produces a gradual transfer of the applied stress to the soil skeleton and consequent increase in effective stress. The dissipation of excess pore-water pressure, also referred to as "hydrodynamic lag" by Terzaghi (1943), is key to understanding the consolidation process.

Mathematical consolidation theory describes the dissipation of excess pore-water pressure and associated volume change of the soil. The underlying assumptions of Terzaghi's (1943) classical consolidation theory include: (1) soil is saturated; (2) Darcy's law is valid; (3) the relationship between void ratio and effective stress is one-to-one and linear; and (4) soil properties such as hydraulic conductivity and compressibility remain constant. There have been extensive investigations of consolidation behavior for saturated soils over the many subsequent decades to account for large strains (Gibson et al. 1967; Fox and Berles 1997), layered soils (Fox et al. 2014), accreting layers (Fox 2000), vertical and radial flows (e.g., Fox et al. 2003), constant rate of strain (Wissa et al. 1971; Pu et al. 2013), soil self-weight (Gibson et al. 1981; Bonin et al. 2014), secondary compression (i.e., creep) effects (Brandenberg 2015), coupled solute transport (Fox 2007a, b), electroosmosis (Deng and Zhou 2015), and varying hydraulic conductivity and compressibility and non-Darcian flow (Indraratna et al. 2016).

Soils under unsaturated conditions involve three phases and introduce substantial complexity to the consideration of volume change behavior. An instantaneously applied stress is not fully carried by incompressible water and will partially transfer to the soil skeleton and the highly compressible air phase, causing an instantaneous settlement and increase in effective stress. On the other hand, deformation of the soil skeleton may be resisted by soil hardening due to the effects of capillarity and adsorption through suction stress (Lu and Likos 2004), where the capillary effect is mainly due to the surface tension on the curved air–water interface, and adsorption is induced by physicochemical interactions such as van der Waals and electric double-layer forces. In this case, all the physicochemical and capillary forces at or near soil particle contacts in unsaturated soils have been conceptualized and defined as a stress called suction stress. Suction stress, as fully defined by Lu and Likos (2006), is the effective stress due to changes in soil water content. Additionally, depending on initial and loading conditions, unsaturated soils may undergo transition points where air will be expelled or fully dissolved to cause pressurized saturation prior to the onset of particle crushing or void closure at high external stress (Mun and McCartney 2015).

Currently, there are two general methodologies to investigate the hydromechanical coupling effect for consolidation of unsaturated soils: (1) decoupled modeling using independent stress state variables (e.g., Fredlund and Hasan 1979; Lloret and Alonso 1980); and (2) coupled modeling of air and water flow and deformation (e.g., Schrefler and Zhan 1993; Khalili et al. 2000; Conte 2004). Volume change due to environmental loading (i.e., drying or wetting) for expansive soils has received much attention, for instance

[1]Professor, State Key Laboratory of Geomechanics and Geotechnical Engineering, Institute of Rock and Soil Mechanics, Chinese Academy of Sciences, Wuhan, Hubei 430071, PR China. Email: ydong@whrsm.ac.cn

[2]Professor, Dept. of Civil and Environmental Engineering, Colorado School of Mines, Golden, CO 80401 (corresponding author). ORCID: https://orcid.org/0000-0003-1753-129X. Email: ninglu@mines.edu

[3]Shaw Professor and Head, Dept. of Civil and Environmental Engineering, Pennsylvania State Univ., University Park, PA 16802. Email: pjfox@engr.psu.edu

Note. This manuscript was submitted on August 14, 2019; approved on April 6, 2020; published online on July 8, 2020. Discussion period open until December 8, 2020; separate discussions must be submitted for individual papers. This paper is part of the ***Journal of Geotechnical and Geoenvironmental Engineering***, © ASCE, ISSN 1090-0241.

the Clod test (e.g., Krosley et al. 2003); however, the effect of interparticle stress on volume change due to soil desiccation, without the compounding effects of external stress change, has not been exclusively investigated. Although various one- or three-dimensional consolidation models incorporate matric suction as a primary state variable (e.g., Fredlund and Hasan 1979; Lloret and Alonso 1980; Gens and Alonso 1992; Sheng et al. 2008; Zhou et al. 2012), most fail to identify differences between isotropic soil shrinking/swelling under homogeneous drying/wetting conditions (i.e., homogeneous suction stress) and nonisotropic stress under condition of either one- or three-dimensional consolidation caused by external loadings. Previous studies using the drying cake technique have indicated that interparticle stresses or suction stress directly impact soil mechanical properties [e.g., small-strain or finite strain modulus (Dong and Lu 2016a, b; Dong et al. 2016, 2018)], and suction stress is closely related to the soil water retention curve (SWRC) (Lu and Likos 2006; Lu et al. 2010) and soil shrinkage curve (SSC) (Lu and Dong 2017a; Chen and Lu 2018). Therefore, the concept of suction stress provides a better basis on which to interpret the intrinsic volume change of soil induced by drying or wetting alone.

This paper presents experimental results and analysis of soil cake drying tests that are free of external stress or total stress, where suction stress is the only mechanical stress affecting deformation. The shrinkage behavior of soil by suction stress under drying conditions is defined as drying-induced consolidation (DC). Drying-induced consolidation can occur in many field environments such as geosynthetic clay liners for waste isolation and shallow ground in silty and clayey levees and dams. Independent experimental results of fundamental properties, i.e. specific surface area (SSA) and cation exchange capacity (CEC), and practical geotechnical index parameters, i.e., Atterberg limits, are connected through drying-induced consolidation behavior and these connections reveal intrinsic correlations among the SWR, SSC, and DC relationships. The interpretation of drying-induced consolidation provides insights into soil volume change behavior and further verifies the validity and efficacy of a suction stress-based effective stress framework for unsaturated soils.

Consolidation and Soil Shrinkage

Consolidation behaviors for saturated soils are characterized by nonlinear volumetric response to external loading, including the preconsolidation effect of stress history and time-dependent settlement due to excess pore-water pressure dissipation. The transfer of applied total stress from excess pore-water pressure to effective stress acting on the soil skeleton is the cause of soil deformation in the case of saturated soils. However, under unsaturated conditions, soils can develop another type of effective stress depending on water content and soil type. Fig. 1(a) illustrates the concept of passive effective stress and active effective stress in a soil skeleton under external loading and environmental loading, respectively. Passive effective stress occurs due to applied external stress and is a transferable, boundary-condition-dependent global stress in soil, which can be explicitly calculated using total stress and pore-water pressure if soils are fully dry or saturated (e.g., Terzaghi 1943; Santamarina et al. 2001). Active effective stress, e.g., suction stress (Lu et al. 2010) or interparticle stress (Wei 2014), on the other hand, occurs in soil under unsaturated conditions due to soil–water interaction or environmental loading, i.e., soil water in equilibrium with ambient pore air humidity. As such, suction stress is a nontransferable and water-potential-dependent local stress around particle contacts (Lu and Likos 2006). Suction stress can be indirectly quantified through shear strength (Lu and Likos 2006), tensile strength (Lu et al. 2009), deformation (Lu and Kaya 2013), or soil water retention curve (Lu et al. 2010).

If a zero external loading or total stress is applied to soil under unsaturated conditions like soil shrinkage testing or many in situ conditions, suction stress is then the only effective stress causing changes in soil stiffness and deformation. In such drying-induced consolidation case, stress and displacement will take place concurrently upon a new suction stress condition. Similar to the diffusion process in saturated consolidation where external stress is sustained initially by incompressible pore water followed by gradually transformation of pore-water pressure to deformable soil skeleton, the drying-induced consolidation process gradually lowers the water potential as the soil water diffuses with evaporation, transforming the soil water potential into the work done by suction stress and soil shrinkage deformation (Lu and Likos 2006). Apparently, the mechanisms of stress transfer in saturated consolidation and energy transfer in drying-induced consolidation differ from each other, but are similar in the water diffusion process. The time dependency of drying-induced consolidation relies on the phase equilibrium between pore water and water vapor through evaporation/condensation processes, which are governed by soil water diffusivity and environmental boundary conditions.

To extend the concept of soil consolidation behavior to both saturated and unsaturated conditions, Fig. 1(b) shows the change of void ratio in terms of passive and active effective stresses. When a saturated normally consolidated soil experiences volumetric compression, the void ratio gradually decreases and follows a linear normal consolidation line (NCL) with the increase of passive effective stress σ' $(= \sigma - u_w)$ on the logarithmic scale, in the plane of e versus $\log(\sigma')$, where σ is total stress and u_w is pore-water pressure. The slope of the NCL is defined as the compression index C_c for one-dimensional consolidation. When soil experiences unloading from the NCL (i.e., stress removal), a preconsolidation stress is created, and the soil deforms more or less elastically. The void ratio increases according to a smaller recompression index C_r for unloading/reloading, and then returns to the NCL if loading continues beyond the preconsolidation pressure. This relationship of void ratio versus effective stress characterizes volume change for saturated soils under incremental loading at the end of each consolidation stage. In this case, effective stress σ' is passively transferred from the boundary conditions to the soil skeleton.

When soil is unsaturated, an active and nontransferable local stress is developed at particle contacts, termed suction stress. Suction stress is independent of external loading but highly controlled by water content through physicochemical interactions of soil particles such as water adsorption and capillary mechanisms (Lu and Likos 2004, 2006; Lu 2016). When a soil is under environmental loading solely (i.e., drying/wetting processes), shrinkage and swelling occur from changes in suction stress similar to volume change in saturated soils due to external loading. Soil volume change due to suction stress σ^s change under a zero total stress condition is defined herein as the drying-induced consolidation curve (DCC) illustrated in Fig. 1(b) in the plane of e versus $\log(-\sigma^s)$. The negative sign of suction stress indicates it applies tension on the particle surfaces and thus pulls the particles together. Because of the isotropic nature of matric suction (Lu and Likos 2004, p. 38), suction stress isotropically consolidates an isotropic soil during a homogenous drying or wetting process.

The DCC under drying follows a compression line with slope C_c^s, which is defined as the compression index of drying-induced consolidation [Fig. 1(b)]. The rebound of the void ratio under wetting follows an unloading/recompression line with smaller slope C_r^s, which is defined as the recompression index of drying-induced consolidation. Compared with consolidation by passive effective

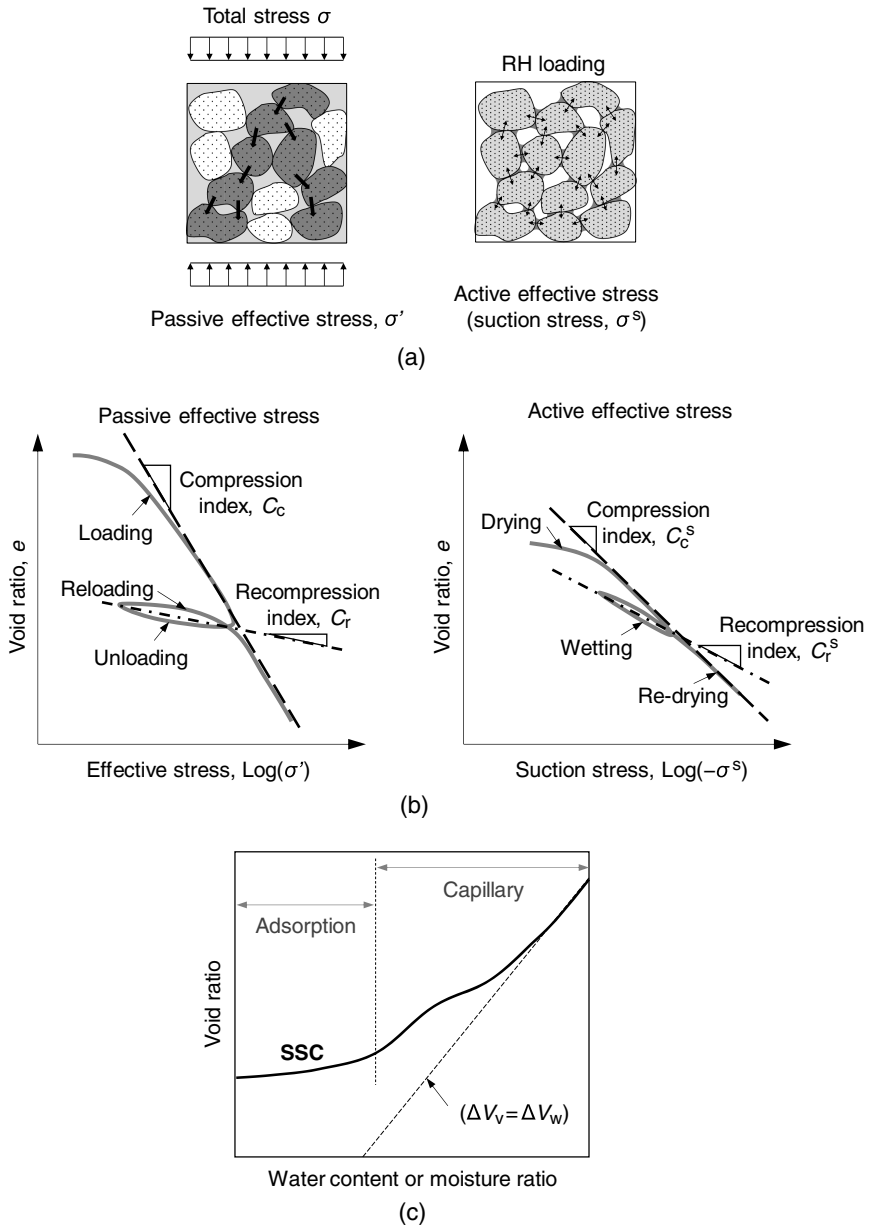

Fig. 1. Illustration of consolidation and shrinkage characteristics: (a) difference between passive and active effective stress in soil skeleton; (b) consolidation by passive and active effective stress; and (c) typical soil shrinkage curve.

stress under saturated conditions, C_c^s and C_r^s have much lower values and are closer in magnitude. This occurs under drying and wetting due to the slight hysteresis of volume change in the low water content or high suction range (Dong and Lu 2017). Some studies (e.g., Wheeler et al. 2003) showed that irreversible plastic deformation occurs in soils under both hydraulic and mechanical processes. However, soils can elastically deform along drying and wetting paths under a zero-external-stress condition after air entry, and plastic deformation only occurs in the funicular soil water retention regime (Fleureau et al. 1993, 2002).

In a previous study on soil shrinkage behavior, Lu and Dong (2017a) proposed a new conceptual model for soil volume change. Fig. 1(c) shows a typical SSC as represented by the relationship between void ratio and moisture ratio, where moisture ratio is defined as the ratio of volume of water to volume of solid. The dashed line indicates the condition of soil volume change equal to water volume change (i.e., saturated soil). SSC can be conceptually divided into two parts: a capillary state and an adsorptive state (Lu and Dong 2017a). As the soil dries from a saturated condition, the void ratio first decreases along the dashed line until air entry occurs and the soil becomes unsaturated. At this point, the SSC begins to deviate from the dashed line, and the incremental volume change of voids is less than the incremental volume change of water. On continued drying, the SSC passes out of the capillary state, and the slope continues to decrease. Although the adsorption state and capillary state may overlap, the boundary of these two states on Fig. 1(c) can be estimated as the point where the slope of the SSC transitions to a smaller value (indicated by the vertical dash line). The new SSC conceptual model defines different shrinkage states based on SWR behavior and identifies the nonzero shrinkage rate of expansive soil in the tightly adsorbed (i.e., low water content) state. The SSC also provides a new perspective from which to calculate suction stress for soils under unsaturated conditions, especially at the low-water-content range.

Table 1. Geotechnical properties of seven soils

No.	Soil	Expansive soil classification[a]	USCS	Porosity,[b] n	Atterberg limits			References
					LL (%)	PL (%)	PI	
1	BoS	Low-expansive	ML	0.417	25	21	4	Lu and Dong (2017a)
2	BaS	Low-expansive	ML	0.458	27.4	21.7	5.8	Lu and Dong (2017a)
3	IaS	Low-expansive	ML	0.492	33.7	22.4	11.3	Lu and Dong (2017a)
4	ZzS	Low-expansive	ML	0.446	27.5	15.5	12.0	Current study
5	GaK	Non-expansive	MH	0.522	44	26	18	Lu and Dong (2017a)
6	MoC	Expensive	CL	0.490	36	17	19	Lu and Dong (2017a)
7	SmC	Expansive	CL	0.484	36.2	19.4	16.8	Current study
8	DCs	Expensive	CL	0.471	44	23	21	Lu and Dong (2017a)
9	BoC	Expensive	CL	0.435	41	18	23	Current study
10	DcDb	Expensive	CL	0.581	81[c]	34[c]	47	Current study
11	DBt	High-expansive	CH	0.692	118	45	73	Lu and Dong (2017a)
12	NmC	High-expansive	CH	0.567	218	58	160	Current study

Note: BoS = Bonny silt; BaS = Bay area landslide silt (or Bay area landslide silt); IaS = Iowa silt; ZzS = Zhengzhou silt; GaK = Georgia kaolinite; MoC = Missouri clay; SmC = Sanmenxia clay; DCs = Denver claystone; BoC = Boulder clay; DcDb = mixture of Denver claystone and Denver bentonite; DBt = Denver bentonite; and NmC = Ningming clay.
[a]According to the method by McKeen (1992).
[b]Initial porosity under saturated condition.
[c]Data calculated using interpolation by mass fraction.

Experimental Program and Soil Properties

To investigate the deformation response of unsaturated soils during drying-induced consolidation, an experimental program was conducted on various silty and clayey soils, and in addition, relevant data were included from current and previous studies. Results and analysis of suction stress and drying-induced consolidation behavior are presented in the current paper.

Geotechnical Properties

Experimental data from 12 fine-grained soils were used for the current study, as described in Table 1. The Unified Soil Classification System (USCS) classifications cover the range of fine-grained soils, including ML (silt of low plasticity), MH (silt of high plasticity), CL (clay of low plasticity), and CH (clay of high plasticity). According to the McKeen (1992) expansive soil classification, the soils are (1) nonexpansive clay Georgia kaolinite (GaK); (2) low-expansive silt including Bonny silt (BoS), Bay area landslide silt (BaS), Iowa silt (IoS), and Zhengzhou silt (ZzS); (3) expansive clay including Missouri clay (MoC), Denver claystone (DCs), Sanmenxia clay (SmC), Boulder clay (BoC), and the mixture of Denver claystone and Denver bentonite (DcDb); and (4) high-expansive clay including Denver bentonite (DBt) and Ningming clay (NmC). Atterberg limits of these soils range from: $25 < LL < 218$, $17 < PL < 58$, and $4 < PI < 60$ (LL = liquid limit; PL = plastic limit; and PI = plasticity index). For the mixture of Denver claystone and Denver bentonite, LL and PL can be estimated by linear interpolation based on the mixture composition, according to Sharkey (2002).

CEC and SSA Measurements

The SSA and CEC of eight soils were available from some previous studies, obtained using a SWR-based methodologies described by Khorshidi and Lu (2016) and Khorshidi and Lu (2017), respectively, and are summarized in Table 2. The soil water adsorption isotherms were measured using a vapor sorption analyzer (VSA)

Table 2. SWR parameters, surface properties, and compression index for the examined soils

No.	Soil	SWRC model parameters[a]			Surface properties		Compression index, C_c^s	Power of modulus[d], p
		α (kPa^{-1})	N	θ_a^{max}	SSA[b] (m^2/g)	CEC[c] (meq/g)		
1	BoS	0.027	1.53	0.024	111.94	0.21	0.037	1.26
2	BaS	0.059	1.72	0.024	76.16	0.24	0.034	1.52
3	IaS	0.083	1.55	0.046	104.09	0.22	0.047	1.08
4	ZzS	—	—	—	—	—	0.028	0.90
5	GaK	0.004	1.86	0.009	28.26	0.09	0.111	2.18
6	MoC	0.083	1.35	0.081	299.8	—	0.085	2.26
7	SmC	—	—	—	—	—	0.105	1.34
8	DCs	0.010	1.56	0.111	152.64	0.35	0.143	1.64
9	BoC	—	—	—	—	—	0152	0.79
10	DcDb	0.012	1.51	0.132	406.18[e]	0.52[e]	0.298	2.11
11	DBt	0.014	1.41	0.156	659.72	1.69	0.498	1.79
12	NmC	—	—	—	—	—	0.577	3.15

[a]SWRC model of Lu (2016).
[b]Data from Khorshidi and Lu (2016).
[c]Data from Khorshidi and Lu (2017).
[d]Data from Young's modulus model of Lu and Kaya (2014).
[e]Data calculated using interpolation by mass fraction.

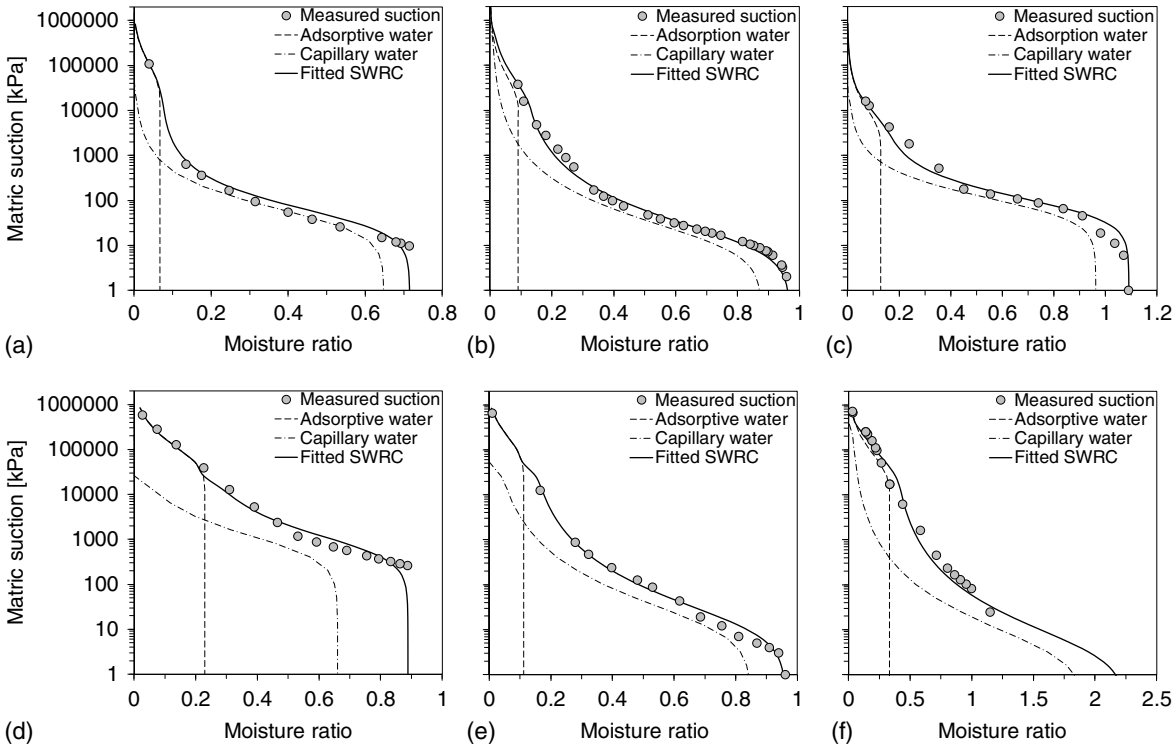

Fig. 2. Typical SWRCs for expansive soils with distinction of capillary and adsorptive water. (Data from Lu 2016.)

(Decagon, Pullman, Washington). The adsorption mechanisms revealed that soil water adsorption consists of cation adsorption and particle surface adsorption (Lu and Khorshidi 2015). Using the specific moisture capacity function (i.e., the change of gravimetric water content due to change of matric potential), the critical points of monolayer or bilayer water molecular coverage associated with particle surface adsorption can be identified from the measured soil water sorption isotherms or SWRCs for adsorption and desorption of soils in the high suction range. The mass of adsorbed water at monolayer gives a total surface area for adsorption sites. The SSA results show close agreement with other independent measurements for the same soils using the conventional ethylene glycol monoethyl ether (EGME) method (Akin and Likos 2014) and other SWR-based methods (Khorshidi and Lu 2016).

Similarly, the SWR model quantifies the interaction of interlayer exchangeable cations and adsorbed dipoles of water molecules and provides an approach to calculate the charge-dipole energies, and correspondingly, the quantity of cations or CEC from the hydration numbers of each cation type (Khorshidi and Lu 2017). Comparison studies have indicated that CEC values obtained from the SWR-based model are in close agreement with those obtained from the conventional ammonium acetate method. In the current study, SSA and CEC data for the eight soils in Table 1, as obtained from independent methods using the SWR model, are used to evaluate the correlation between drying-induced consolidation and SWR behaviors.

SWRC Measurement and Model

The SWRC measurements were conducted in previous studies; the SWRC data for Bonny silt, Georgia kaolinite, and Denver claystone have been presented by Dong and Lu (2017), and the SWRC data for Bay area landslide silt, Iowa silt, Missouri clay, and Denver bentonite were presented by Dong and Lu (2016a). The mixture of Denver claystone and bentonite with a 1:1 mass ratio was tested in that paper. To cover a full range of matric suction, including high suction conditions, SWRCs for these eight soils were obtained by combining results from the transient water release and imbibition method (Wayllace and Lu 2012) for the low regime, and results from the vapor sorption isotherm technique (Likos et al. 2011) for the high regime. Fig. 2 presents the resulting SWRCs for 6 soils, including low-expansive, nonexpansive, expansive, and high-expansive soil types.

The recent SWRC model of Lu (2016) emphasizes the difference between capillary water and adsorptive water, with considerations of the upper bound of adsorption (i.e., highest matric suction) and the limit of capillarity (i.e., cavitation suction) to fully describe the SWR behavior for all soils. This model expresses the total volumetric water content $\theta(\psi)$ as the sum of adsorptive water content $\theta_a(\psi)$ and capillary water content $\theta_c(\psi)$ in equilibrium with the prevailing matric suction ψ

$$\theta(\psi) = \theta_a(\psi) + \theta_c(\psi) \tag{1}$$

The adsorptive water content is characterized using an adsorption model by Lu (2016)

$$\theta_a(\psi) = \theta_a^{\max}\left\{1 - \left[\exp\left(1 - \frac{\psi_{\max}}{\psi}\right)\right]^M\right\} \tag{2}$$

where $\theta_a^{\max}$ = maximum adsorptive water content; M = adsorption strength depending on the soil and cation types; and $\psi_{\max}$ = maximum matric suction (i.e., upper bound). The capillary water is characterized using a modified van Genuchten (1980) SWRC model considering the cavitation effect (Lu 2016)

$$\theta_c(\psi) = \frac{1}{2}\left[1 - \text{erf}\left(\frac{\psi - \psi_{\text{cav}}}{0.25\sqrt{2}\psi_{\text{cav}}}\right)\right](\theta_s - \theta_a(\psi))\{1 + [\alpha\psi]^N\}^{1/N-1} \quad (3)$$

where α and N = inverse of air-entry suction and the pore-size distribution parameters, respectively; and ψ_{cav} = mean cavitation suction where capillary water diminishes or is cavitated. Eqs. (1)–(3) provide a quantitative assessment of adsorptive water and capillary water in terms of seven physically meaningful parameters. The parameters $\psi_{\max}$ and ψ_{cav} are two soil intrinsic properties introduced in the SWRC model of Lu (2016), but are numerically determined in this study by fitting the available experimental soil water retention data. All measured SWRC data were fitted by using the Lu (2016) SWRC model to establish parameter values, and they show close agreement. Some of the key parameters, namely α, N, and $\theta_a^{\max}$, are provided in Table 2. The relative proportions of capillary and adsorptive water are indicated for six soils in Fig. 2.

Deformation and Soil Shrinkage Curve

Volumetric shrinkage of the soils during drying was measured using an improved drying cake technique (Dong and Lu 2017). Soil materials were oven-dried, pulverized, and then saturated with deionized water using a vacuum. The soils were placed as thin soil cakes into plastic specimen containers with an initial diameter of 7.6 cm and initial height of 1.7 cm. The contacting surface of the sample holder was spread with a thin layer of grease to eliminate any friction, adhesion, or deformation constraints. The specimens then were placed in an environmentally controlled humidity chamber and were dried by evaporating slowly over a period of 2–3 weeks, ensuring uniform soil moisture distribution within the specimen in order to avoid soil cracking. During drying, changes of specimen diameter were recorded using a digital camera and analyzed by image processing, and changes of specimen thickness were measured using the miniloading system described by Dong and Lu (2017). For homogeneous soils, horizontal strains in orthogonal radial directions and vertical strain over specimen thickness each contribute about one-third of the total volumetric strain. Variations in these strains can also be used to assess heterogeneity in moisture distribution and anisotropy in suction stress development during the drying process.

A data set of 12 soil shrinkage curves are collected in this paper. Among those, BoS, BaS, IaS, GaK, MoC, DCs, and DBt are from Lu and Dong (2017a), and the remaining five soils (ZzS, SmC, BoC, DcDb, and NmC) are measured in this study. Nine selected shrinkage characteristic curves are presented in Fig. 3 and indicate volume change behavior that varies greatly with soil type. Silty soils experience a relative small fraction (approximately 10%–25%) of total volume change, e.g., Bonny silt shrinks 24% from a void ratio of 0.72 to 0.55, Iowa silt shrinks 15% from 0.97 to 0.82, and Zhengzhou silt shrinks 11% from 0.81 to 0.72. In contrast, expansive clays experience larger (approximately 30%–40%) volume change: 29% from 0.76 to 0.54 for Sanmenxia clay, 32% from 0.97 to 0.66 for Missouri clay, and 35% from 0.77 to 0.32 for Boulder clay. High-expansive soil present significant (larger than 50%) volume change, e.g., 53% from 0.89 to 0.42 for Denver claystone, 66% from 2.23 to 0.75 for Denver bentonite, and the largest volume change 67% from 1.31 to 0.43 occurs for Ningming clay.

Fig. 3 also indicates that the pattern of shrinkage varies at different soil water regimes for the different soils. The dashed line in each plot represents a saturated condition where changes in void ratio are equal to changes in moisture ratio. For nonexpansive clay, Georgia kaolinite reduces almost 95% of the entire volume in the saturated condition (i.e., capillary stage) when the moisture ratio is higher than 0.75. However, for silty soil, Bonny silt, Iowa silt, and

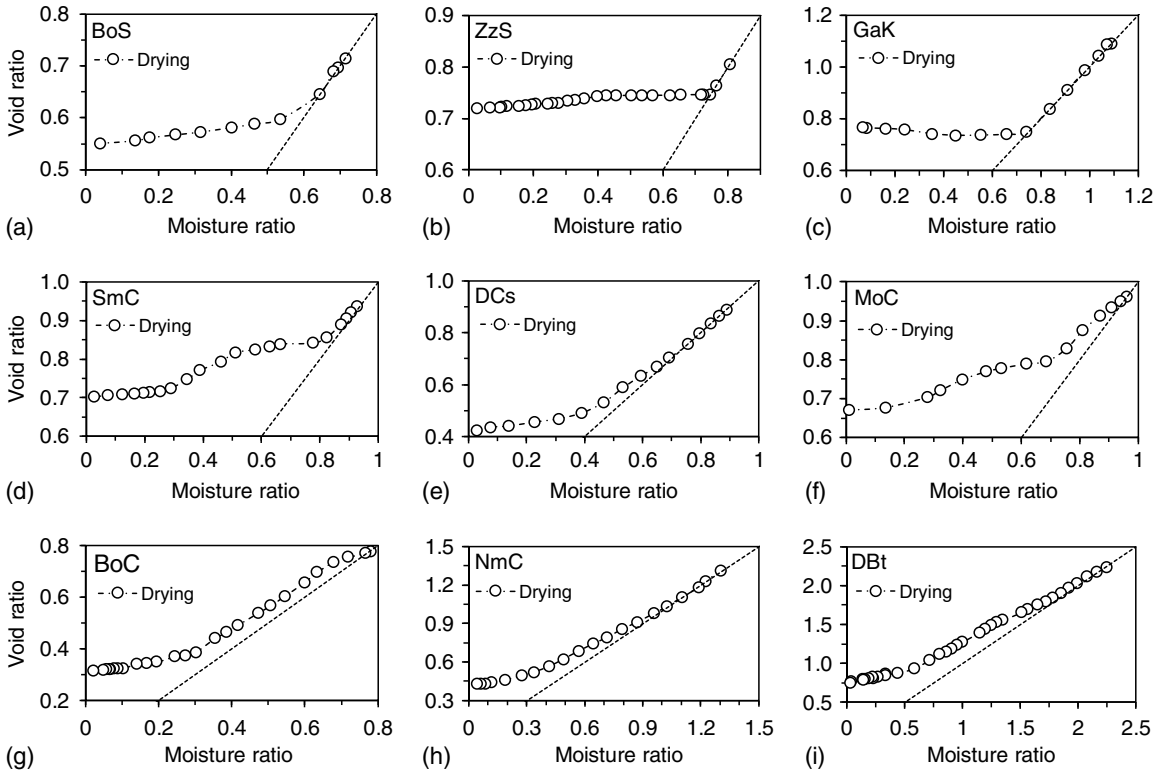

Fig. 3. Comparisons of the measured void ratio variations.

Zhengzhou silt undergo 47%, 33%, and 48% of the shrinkage before the air entry into the soil matrix. For expansive clay, Denver claystone, Missouri clay, Boulder clay, and Sanmenxia clay experience as large as 70%–95% of the total volume shrinkage after the point of air entry (70%, 93%, 95%, and 73%, for DCs, MoC, BoC, and SmC, respectively). For high-expansive soil, Denver bentonite and Ningming clay show the relatively high level of 85% and 90% of total shrinkage beyond the air entry point. After the capillary and pendular stages, silty soils do not experience significant total volume change in the adsorption water regime due to lack of clay content and thus the shrinkage rate is small. Conversely, the expansive clays retain 25%–35% shrinkage capacity in the adsorption water retention regime.

Drying-Induced Consolidation Behavior

The determination of suction stress is the key to the analysis of drying-induced consolidation. Two deformation-based calculations were conducted independently to compare the suction stress: a linear elasticity solution consistent with the plane-stress conditions imposed by the particle image velocimetry (PIV) process (Lu and Kaya 2013; Lu and Dong 2019), and a new bulk volume solution consistent with the more general volumetric strain conditions for the DCC analysis. The drying cake method employs the stress-strain relationship described by the effective stress. Although soil stiffness and deformation are highly nonlinear and could be inelastic in general, an incremental linear elasticity within small range of stress and strain variation has been used and was validated for the suction stress calculation in previous studies (Lu and Kaya 2013; Dong and Lu 2017). Its working principle is that the effective stress due to water content change (suction stress) can be determined by strain and modulus using linear elasticity at a given soil water content for a small increment of moisture change. An analytical solution can be obtained by extending the classical linear elasticity into a suction-stress-based effective stress problem. Specifically, the force equilibrium equations under a polar coordinate system are applied, leading to solutions of suction stress and soil deformation (displacement) (Lu and Kaya 2013; Lu and Dong 2019)

$$\sigma^s(\theta) = -\frac{E(\theta) \cdot u_r(r,\theta)}{(1-2\nu) \cdot r(\theta)} \tag{4a}$$

or

$$u_r(r,\theta) = -\frac{(1-2\nu) \cdot r(\theta) \cdot \sigma^s(\theta)}{E(\theta)} \tag{4b}$$

where $\sigma^s(\theta)$ = suction stress at the volumetric water content θ; $u_r(r,\theta)$ = water-content-dependent radial displacement at a distance (r) from the center of the displacement field center; $E(\theta)$ = water-content-dependent elastic modulus of soil; and ν = Poisson's ratio of soil.

For each analysis method, the elastic soil modulus is needed at various water contents to calculate suction stress. Values of elastic modulus were measured for a replicate specimen (i.e., prepared identically with the drying cake specimen for the PIV measurement) using a miniloading system to record the vertical stress and strain (Dong and Lu 2017). For these tests, the loading actuator applies a small vertical displacement rate (<0.25 μm/s) to the top of the specimen without any lateral stress constraint and measured the associated vertical stress up to a maximum vertical strain of 1% at various water contents. The small strain limit is used to approximately satisfy the assumption of reversible elastic deformation and uniform distribution of soil moisture (and hence suction) inside the soil cake. A power law function for elastic modulus (Lu and Kaya 2014) was used to fit the measured data

$$\frac{E_{\text{dry}} - E}{E_{\text{dry}} - E_{\text{wet}}} = \left(\frac{\theta - \theta_{\text{dry}}}{\theta_{\text{wet}} - \theta_{\text{dry}}}\right)^p \tag{5}$$

where E_{dry} and E_{wet} = values of elastic modulus at dry (θ_{dry}) and wet (θ_{wet}) states, respectively; and p = fitting parameter. In the current study, the wet state is the fully saturated condition and the dry state is the equilibrium moisture condition for the relative humidity in the test room (~15%). Least-squares regression was used to fit Eq. (4) with the measured elastic modulus data, and the resulting p values for all 12 soils are provided in Table 2.

Fig. 4 compares the measured modulus data and fitted power law relationships for six soils. In each case, the elastic modulus increases as the moisture ratio decreases during the drying process, and close agreement is observed.

Suction Stress from Plane-Stress Method

The linear elasticity solution for the plane-stress method requires values of radial displacement $u_r(r,\theta)$ and displacement center $r(\theta)$, as described by Lu and Kaya (2013). The radial displacement field and displacement center are obtained from digital still camera images and subsequent image processing using PIV software (White et al. 2003). Images of the soil cake were discretized using a regular grid, and the vector displacement field of each element patch and the displacement center of entire mesh were identified progressively during the drying process. Fig. 5(a) shows an example for Georgia kaolinite during the drying process, where displacement vectors and the displacement center are indicated for one incremental step in volumetric water content θ. The magnitude of each displacement vector is proportional to the distance from the target point to the displacement field center. Longer displacement vectors can be observed for points away from the displacement center or closer to the edge of the soil cake. The radial strains ($\varepsilon_r = \partial u_r/\partial r$) obtained at each local point are nearly identical, confirming the assumption of homogeneous deformation throughout the cake sample. As the soil dries, the volume decreases, and the displacement arrows point inward; the displacement center represents the location where no displacement occurs (Lu and Dong 2017b). The corresponding incremental suction stress $\Delta\sigma^s$ for the same incremental step can be derived from Eq. (4*a*) as follows (Lu and Dong 2019):

$$\Delta\sigma^s(\theta) = -\frac{u_r(r,\theta)}{(1-2\nu) \cdot r(\theta)}\Delta E(\theta) - \frac{E(\theta)}{(1-2\nu) \cdot r(\theta)}\Delta u_r(r,\theta) + \frac{E(\theta) u_r(r,\theta)}{(1-2\nu) \cdot r^2(\theta)}\Delta r \tag{6}$$

where Poisson's ratio v is assumed to be 0.25 for all soils (Lu and Kaya 2013). Eq. (6) applies for suction stress at each point or every discretized element of PIV mesh on the soil cake surface at any water content level. The overall suction stress for every drying step can be obtained by the average of all local suction stresses. Fig. 5(b) demonstrates images of shrinkage for highly expansive Ningming clay at various water contents.

Suction Stress from Bulk-Volume Method

Alternatively, assuming that the soil dries homogeneously and the isotropic suction stress is uniform at any time, the soil cake can represent a soil element and therefore the suction stress

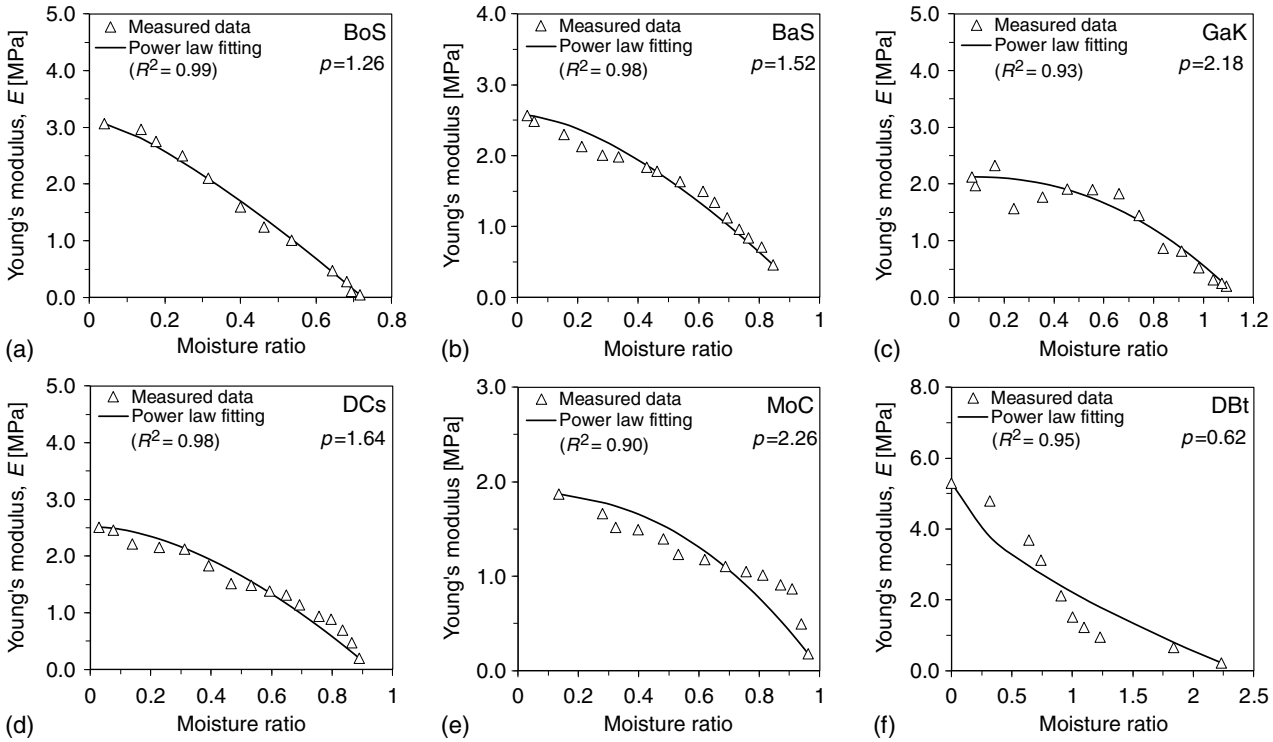

Fig. 4. Elastic modulus variations with volumetric water content: (a) Bonny silt; (b) Bay area landslide silt; (c) Georgia kaolinite; (d) Denver claystone; (e) Missouri clay; and (f) Denver bentonite.

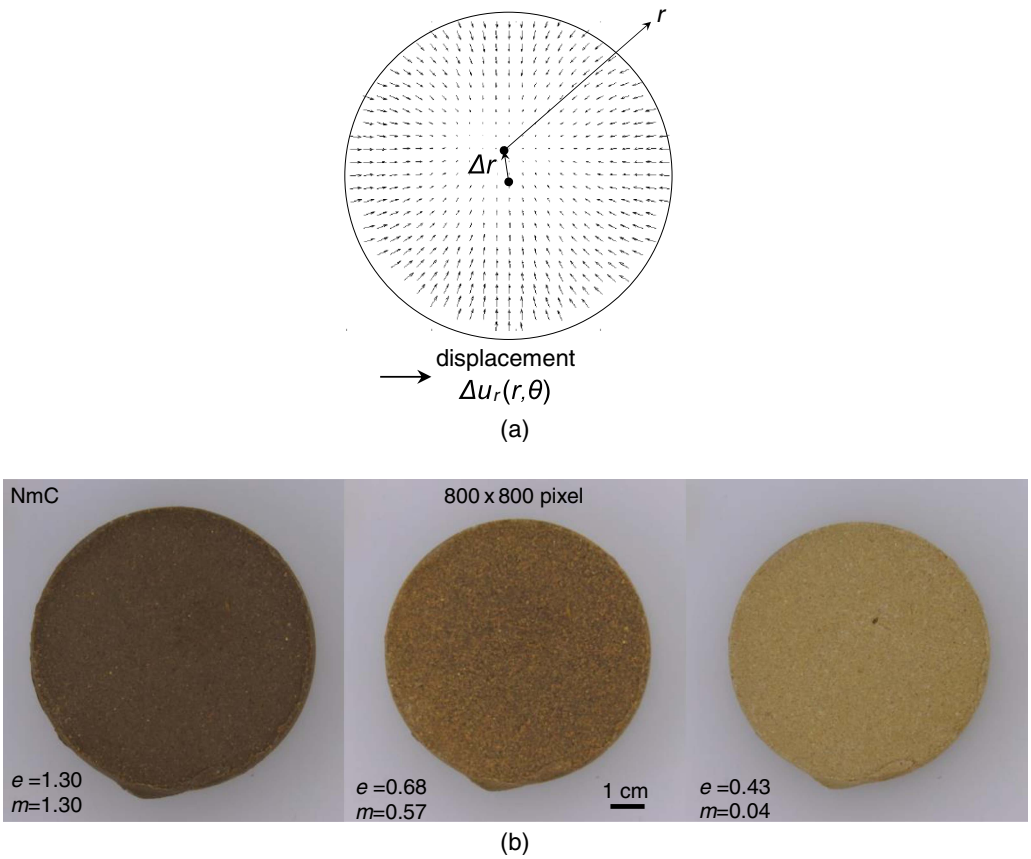

Fig. 5. Typical shrinkage of soil cake sample under drying: (a) radial displacement $u_r(r,\theta)$ and displacement field center $r(\theta)$ in the plain-stress solution under the radial coordinate system during shrinkage of Georgia kaolinite at volumetric water content θ; and (b) the soil cake sample (Ningming clay) with varying volume at different moisture ratios.

characteristic curve (SSCC) can be directly deduced from the measured $E(\theta)$ and SSC relationships. The total volumetric strain ε_v of the drying soil cake is

$$\varepsilon_v = \Delta V/V \tag{7}$$

and the relationship between the volumetric strain and change in void ratio is

$$\Delta e = \varepsilon_v/(1-n) \tag{8}$$

Assuming soil moisture is homogeneous at any point during the drying process, strains and suction stresses developed with in the soil cake are isotropic (i.e., equal in all directions)

$$\varepsilon_v = 3\varepsilon_z = 3\varepsilon_r \tag{9}$$

$$-\sigma^s = \sigma_z' = \sigma_r' \tag{10}$$

where ε_z and ε_r = vertical and radial strains; and σ_z' and σ_r' = vertical and radial stresses, respectively. According to elastic theory, vertical strain of the soil cake can be expressed as follows (Lu and Kaya 2013):

$$\varepsilon_z = \frac{\sigma_z'}{E} - \nu\frac{\sigma_x' + \sigma_y'}{E} = \frac{\sigma_z'}{E} - \nu\frac{2\sigma_r'}{E} = \frac{\sigma^s}{E}(2\nu - 1) \tag{11}$$

Rearranging Eq. (11) and substituting ε_z by ε_v by Eq. (9), the suction stress is

$$\sigma^s = \frac{E \cdot \varepsilon_v}{3(2\nu - 1)} \tag{12}$$

and the incremental form of suction stress is

$$\Delta\sigma^s = \frac{E}{3(2\nu-1)}\Delta\varepsilon_v + \frac{\varepsilon_v}{3(2\nu-1)}\Delta E \tag{13}$$

Therefore, the decrease in total suction stress from a wet state can be established by the summation of increments over all volumetric water contents as follows:

$$\sigma^s = \sum_m \Delta\sigma^s = \sum_m \frac{E}{3(2\nu-1)}\Delta\varepsilon_v + \sum_m \frac{\varepsilon_v}{3(2\nu-1)}\Delta E \tag{14}$$

Substituting for total volumetric strain from Eq. (8), the suction stress characteristic curve for drying conditions becomes

$$\sigma^s = \sum_m \Delta\sigma^s = \frac{E}{3(2\nu-1)}\sum_m \Delta(\Delta e(1-n)) + \frac{\Delta e(1-n)}{3(2\nu-1)}\sum_m \Delta E \tag{15}$$

This method calculates suction stress using bulk volumetric strain assuming soil cake sample behavior as a representative elementary volume, which is a key difference from the previous method, which is based on discretized elements. The SSCCs for six soils as calculated independently by the drying cake method [Eq. (5)] and by SSC [Eq. (14)] are compared in Fig. 6.

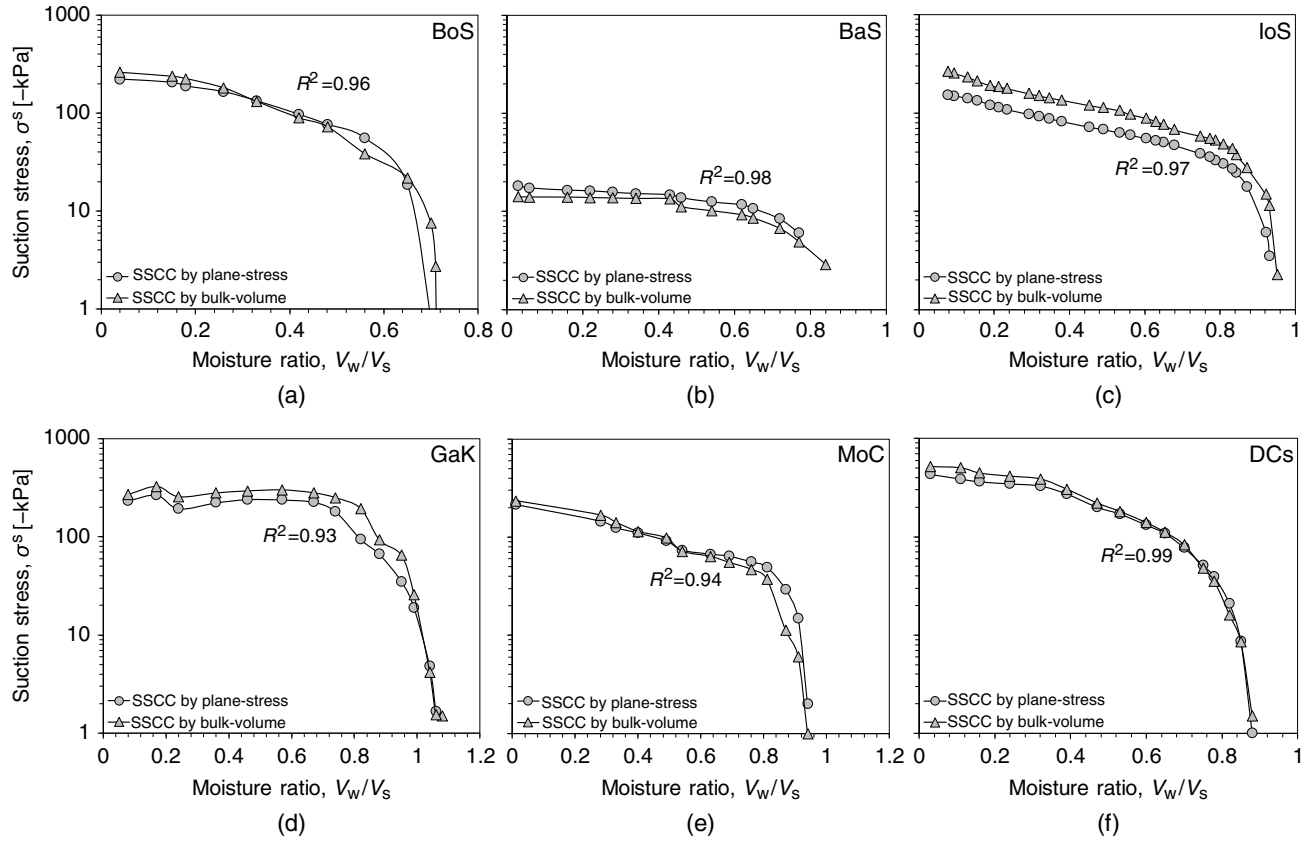

Fig. 6. Comparisons of suction stress characteristic curves by drying cake method and SSC method: (a) Bonny silt; (b) Bay area landslide silt; (c) Iowa silt; (d) Georgia kaolinite; (e) Missouri clay; and (f) Denver claystone.

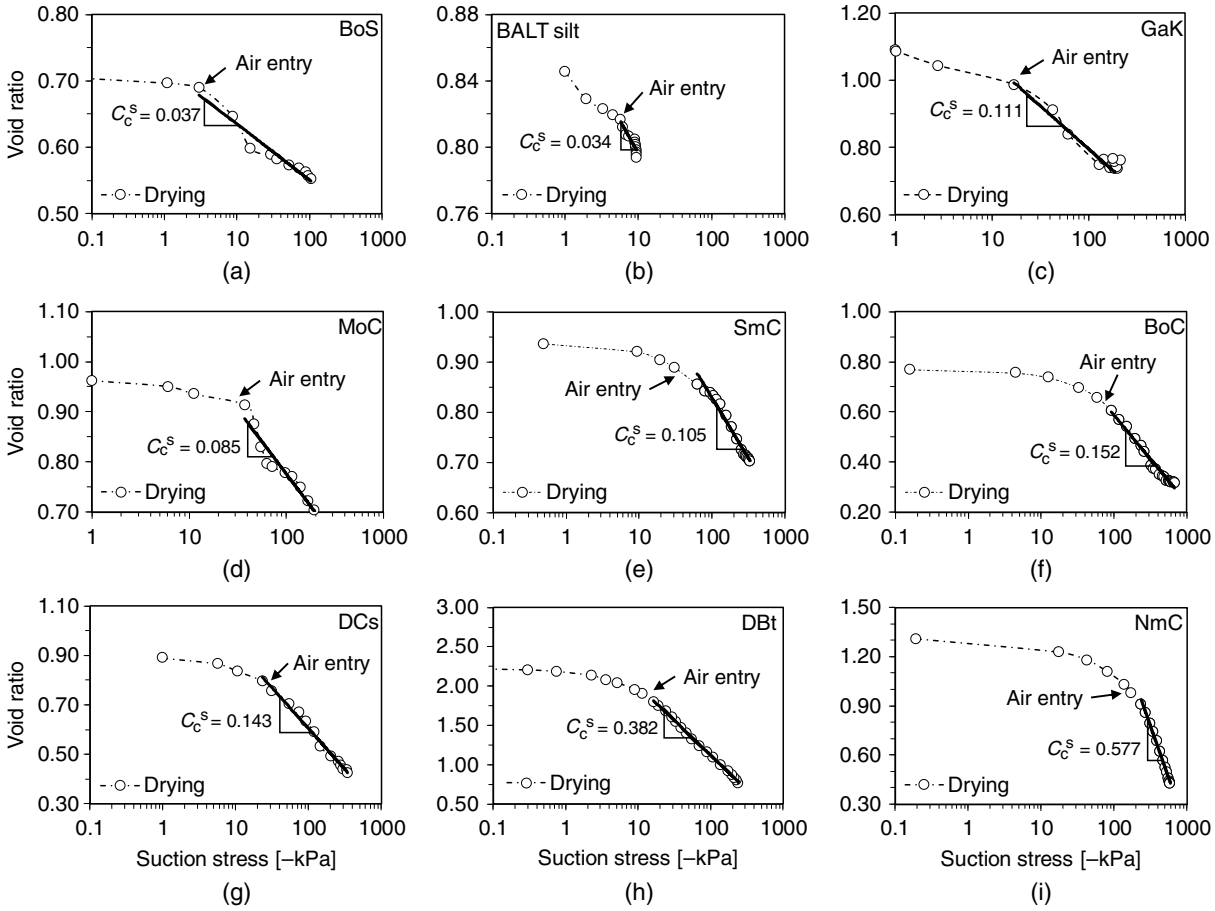

Fig. 7. Drying-induced consolidation curves by suction stress for different soils.

Suction stress generally decreases as the soil dries due to the clay content, except for Georgia kaolinite where a slight increase occurred as the soil dries into the adsorptive soil water retention regime. Silty or low-expansive soils can develop suction stress from negative tens of kPa (e.g., around −10 kPa for Bay area landslide silt) to negative hundreds of kPa (e.g., around −100 kPa for Bonny silt) at the dry end, whereas clayey or high-expansive soils have relatively low suction stress (<−300 kPa). The two suction stress solutions are in close agreement for each soil, which validates the effectiveness of the deformation-based suction stress calculation.

Volume Change due to Suction Stress

After the determination of the SSCC for confinement-free drying conditions, the relationship between void ratio and suction stress (i.e., drying-induced consolidation curve) is shown for nine soils in Fig. 7. In the absence of total stress for these thin soil cakes, effective stress is equal to the opposite of suction stress. The plots show generally consistent behavior and, interestingly, some similarity with saturated soil compressibility relationships. The void ratio decreases with decreasing suction stress (i.e., increasing effective stress) and indicates different rates of volume change on the logarithmic scale similar to overconsolidated and normally consolidated stages for saturated soils. Changes in void ratio are small for high suction stress (less negative) and then increase at lower suction stress levels. A transition in slope occurs as the soil begins to become unsaturated (i.e., around point of air entry), and the void ratio changes at a greater rate. At lower suction stress, the plot can be approximated as linear and resembles a normal consolidation line with constant slope C_c^s, which is defined as the compression index for drying-induced consolidation and depends on soil type. Although void ratio and suction stress individually evolve quite nonlinearly with moisture ratio or volumetric water content as the soil dries, as shown in Figs. 3 and 6, respectively, the trend of variation of void ratio becomes essentially linear in terms of suction stress. Fig. 7 also indicates that suction stress plays a critical role for soil deformation due to drying and suggests that suction stress exerts some similar effect on soil deformation as compared with external surcharge loading of saturated soils.

Correlation between DCC and Soil Properties

Values of compression index C_c^s for the seven soils are plotted versus SSA and CEC in Fig. 8. In general, soils with high fines contents, and in particular high clay contents, have higher SSA and CEC values and higher compressibility. For low-expansive silty soils with small SSA (~100 m^2/g) and small CEC (~0.23 meq/g), the compression index is relatively low (~0.05). This is the result of minor adsorption effects due to weak particle surface adsorption and cation adsorption as the soils dry into the adsorptive water retention regime. For nonexpansive clay, such as Georgia kaolinite with SSA < 30 m^2/g and CEC ~ 0.09 meq/g, the adsorption effect is minimal, and most of the volume change occurs in the capillary water retention regime. As the soil dries into the adsorptive regime, the total volume can remain unchanged or even increase as the soil continues to dry. Therefore, the void ratio moves back and forth along the normal consolidation line, as shown in Fig. 7(d), due to the increase or decrease of suction stress. However, the

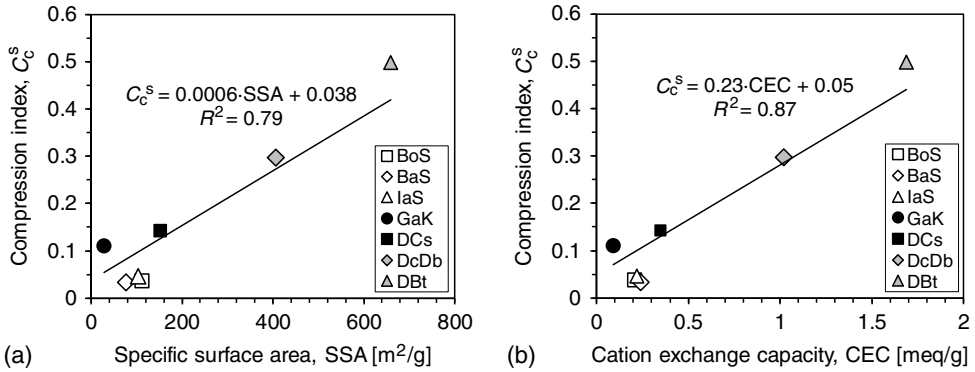

Fig. 8. Correlation of the compression index with SWR characteristics: (a) specific surface area; and (b) cation exchange capacity.

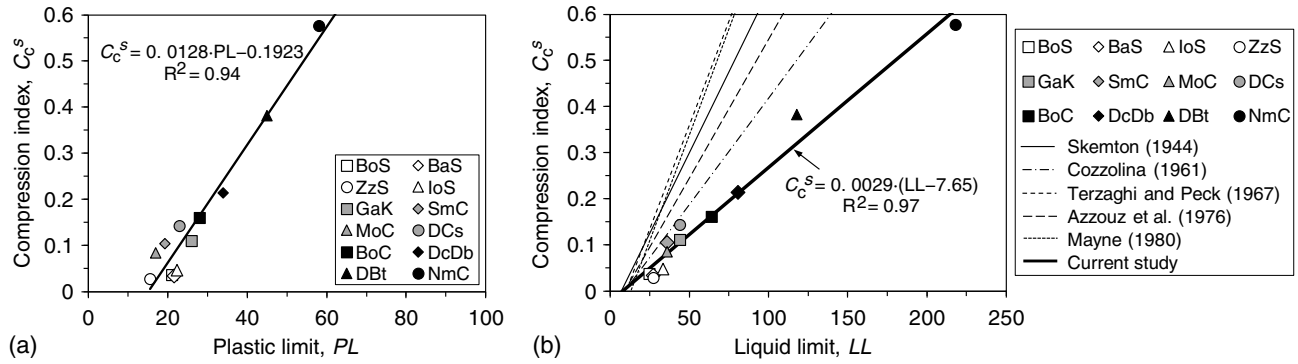

Fig. 9. Correlation of the compression index with Atterberg limits: (a) plastic limit; and (b) liquid limit.

strong capillary effect induced by the small particle size of kaolinite still contributes a moderate compression index ~0.11 for drying-induced consolidation.

For expansive and high-expansive clays, relatively high values of SSA ~ 150–650 m^2/g and CEC ~ 0.4–1.7 meq/g introduce strong effects of particle surface adsorption and cation adsorption, which increases the value of C_c^s as well. The relatively high initial void ratio, indicating large interlayer spaces within particles, provides stronger physicochemical interaction in the adsorption water regime, induces lower suction stress, and further results in large volume shrinkage and compressibility and a high compression index of 0.1–0.5. Although the trend lines show a linear correlation of compression index to SSA and CEC, the experimental data also indicate some scatter. This may explain that suction stress consists of not only the physicochemical forces of adsorption but also capillary forces of the curved air–water interfaces at particle contacts.

Corresponding relationships between compression index and plasticity limit and liquid limit are presented in Fig. 9 and show similar clear and even stronger correlations. Soils with higher PL and LL values tend to experience higher compressibility during drying. For low-expansive silty soils (e.g., Bonny silt, Bay area landslide silt, Iowa silt, and Zhengzhou silt), the PL and LL fall in the ranges of 15.5–22.4 and 25–34, respectively, and yield a compression index around 0.04. For expansive clays, such as Missouri clay, Boulder clay, Sanmenxia clay, and Denver claystone, relatively larger PL and LL values (i.e., 17–23, and 36–44, respectively) yield moderate volume shrinkage and moderate compressibility, with C_c^s ranging from 0.08 to 0.15. For high-expansive clay such as Denver bentonite and Ningming clay, the extremely small particle size and rich exchangeable cations within the particles provide high plasticity with 73 and 160, and high LL values of 118 and 218, respectively, and yield the highest compression index $C_c^s = 0.577$. For a mixture of Denver claystone and Denver bentonite, compression index of drying-induced consolidation shows an average value corresponding to the mixing mass ratio, which is consistent with linearly interpolated values of Atterberg limits of the component soils.

In Fig. 9(b), the correlation between the compression index and LL for drying-induced consolidation of soil due to drying is also compared with the existing correlations found for the traditional consolidation of various soils under saturated conditions (Skempton 1944; Cozzolino 1961; Terzaghi and Peck 1967; Azzouz et al. 1976; Mayne 1980). Each of these previous correlation lines is established for particular or limited range of soil types. Compared with those, the correlation line for drying-induced consolidation presents lower slope and may act as a lower bound for all soil types.

Implications of Drying-Induced Consolidation to Index Properties

The finding of a strong correlation between drying-induced consolidation behavior and index properties invites revisiting of the determination and physical meanings of those index properties, which are often empirically obtained. The liquid limit and plastic limits, which were reckoned by Atterberg over a century ago, are used to define the range of water content in which clay deforms plastically. Qualitatively, higher SSA and CEC values or higher maximum adsorption water content have been well recognized to yield higher LL and PL values. However, no obvious correlations

Table 3. Empirical correlations between compression index and liquid limit

Equation	Applicability	References
$C_c = 0.007(\mathrm{LL} - 7)$	Remolded clays	Skempton (1944)
$C_c = 0.0046(\mathrm{LL} - 9)$	Brazilian clays	Cozzolino (1961)
$C_c = 0.009(\mathrm{LL} - 10)$	Normally consolidated clays	Terzaghi and Peck (1967)
$C_c = 0.006(\mathrm{LL} - 9)$	All clays with LL < 100%	Azzouz et al. (1976)
$C_c = 1/109(\mathrm{LL} - 13)$	All clays	Mayne (1980)
$C_c^s = 0.0029(\mathrm{LL} - 7.65)$	All soils	Current study

have been established directly between fundamental properties reflecting basic soil characteristics (such as SSA and CEC) and index properties reflecting soil bulk strength. The deformation characteristics of soil under confinement-free and drying conditions serve as an intermediate bridge, connecting the two types of properties. Shrinkage and drying-induced consolidation behaviors are not only closely related to soil type and mineral characteristics, but also are determined by bulk properties such as stiffness and strength.

Soil liquid limit, as measured by the Casagrande device to close a soil groove with repeated blows, is associated with an undrained shear strength of approximately 2 kPa (Wood 1990). This test procedure mimics the failure of a miniature soil slope induced by a series of shock decelerations. Numerous previous studies have concluded different empirical relationships between compression index and liquid limit, as listed in Table 3, for saturated conditions. In the current study, the strength of unsaturated soils at various water contents provides a similar correlation with liquid limit using the concept of suction stress. This becomes obvious because suction stress also reflects soil tensile strength. Although the compaction effect is less prominent due to the limit of suction stress (up to several hundred kPa) when compared with external loadings where soil particles can be rotated or crushed, the compression index follows a similar mathematical form, but with a smaller coefficient of linearity than the other empirical equations.

The soil plastic limit is determined by rolling a thread of clay soil until it crumbles into pieces. The water content at plastic limit represents a critical threshold where the soil plasticity is insufficient for continued deformation and remolding. The plastic limit suggests a tensile failure of soil thread and is associated with a strength of approximately 200 kPa (Wood 1990). The break-up of soil threads in the plastic limit test is related to the inhomogeneous distribution of cohesion during rolling and therefore is more related to the adsorption characteristics or suction stress in the adsorption regime. This is probably why the plastic limit test yields less consistent results than the liquid limit test, and why the correlation of drying-induced consolidation index to PL is not as reliable as the correlation to LL.

A comparison of Figs. 8 and 9 indicates that the relationship between compression index and Atterberg limits is stronger than the relationship between compression index and SSA or CEC. This suggests that mineral properties, such as SSA and CEC, are not sufficient to fully describe the deformation behavior of drying-induced consolidation. When using the compression index corresponding to the suction stress plane, the soil stiffness can be incorporated, and therefore, higher R^2 values exist between stiffness-related compression index (C_c^s) and strength-related Atterberg limits (LL or PL). The existence of a quantitative correlation between the compression index and Atterberg limits also suggests new ways to conduct index property tests and new methods for soil classification that move beyond Atterberg limits.

The soil shrinkage test under free external stress and drying conditions is a simple, rapid, and accurate means to measure the soil shrinkage rate and compression index of drying-induced consolidation. Test results have demonstrated the compression index has strong correlations with SWR characteristics and can be quantitatively related to traditional Atterberg limit tests. Soil shrinkage tests or drying-induced consolidation tests involve fewer artificial manipulations, provide greater consistency of results for the same soil, and have better opportunities for rigorous analysis. Further improvements in testing method and analysis based on soil drying-induced consolidation may be possible, including relationships for soil classification.

Summary and Conclusions

In the current paper, shrinkage deformation behavior of unsaturated soil caused by decreases of implicit and active effective stress (suction stress) during drying have been highlighted and distinguished from traditional consolidation deformation behavior where passive effective stress is transferred from external loadings to a saturated soil skeleton. Experimental data were presented from independent measurements of geotechnical index properties, soil mineral properties, soil water retention, and soil shrinkage for various silty and clayey soils. A new deformation-based bulk-volume solution has been derived from the shrinkage curve of a drying soil cake to calculate the suction stress, and the results compare closely with a previously developed linear elastic drying cake (plane-stress) solution. A critical evaluation of volume change behavior under drying conditions has been presented using a suction stress interpretation, with applicability from nonexpansive to high-expansive fine soils. The relationship between void ratio and suction stress of a soil under a zero-total-stress conditions is defined as the drying-induced consolidation curve and shows substantial similarity to traditional consolidation relationships for saturated soils. Also, the compression index of drying-induced consolidation is defined, similarly, as the slope of void ratio versus logarithm of negative suction stress relationship.

In general, drying-induced consolidation shows strong correlations with the soil water retention curve and suction stress characteristic curve. The correlations between compression indices of drying-induced consolidation and soil water retention characteristics such specific surface area and cation exchange capacity indicate that a clayey soil with high SSA and CEC usually yields a high compression index. The linear correlation between drying-induced consolidation compression index and Atterberg limits, particularly LL, is stronger than correlations with SSA or CEC. The discrepancies between these two correlations (i.e., DCC to SSA/CEC and DCC to LL) indicate that SSA/CEC mainly contribute to water adsorption behavior, whereas drying-induced consolidation also involves soils stiffness and strength as reflected by LL. Drying-induced consolidation reflects intrinsic soil volume change behavior during drying and is independent of boundary conditions or external loading. As a bridge linking SWRC/SSCC and Atterberg limits, drying-induced consolidation behavior shows good capability in the quantification of shrinking/swelling potential.

Data Availability Statement

All the experimental data reported are available from the senior or corresponding author.

Acknowledgments

This research was sponsored by National Science Foundation Grant Nos. CMMI-1363315, CMMI-1622781, and CMMI-1902045. In addition, National Natural Science Foundation of China Grant NSFC-51779254 to YD is gratefully appreciated.

References

Akin, I. D., and W. J. Likos. 2014. "Specific surface area of clay using water vapor and EGME sorption methods." *Geotech. Test. J.* 37 (6): 20140064. https://doi.org/10.1520/GTJ20140064.

Azzouz, A. S., R. J. Krizek, and R. B. Corotis. 1976. "Regression analysis of soil compressibility." *Soils Found.* 16 (2): 19–29. https://doi.org/10.3208/sandf1972.16.2_19.

Bonin, M. D., M. Nuth, A.-M. Dagenais, and A. R. Cabral. 2014. "Experimental study on numerical reproduction of self-weight consolidation behavior of thickened tailings." *J. Geotech. Geoenviron. Eng.* 140 (12): 04014068. https://doi.org/10.1061/(ASCE)GT.1943-5606.0001179.

Brandenberg, S. J. 2015. "iConsol.js: JavaScript implicit finite difference code for nonlinear consolidation and secondary compression." *J. Geotech. Geoenviron. Eng.* 17 (6): 04016149. https://doi.org/10.1061/(ASCE)GT.1943-5622.0000843.

Chen, C., and N. Lu. 2018. "Generalized equation for soil shrinkage curve." *J. Geotech. Geoenviron. Eng.* 144 (8): 04018046. https://doi.org/10.1061/(ASCE)GT.1943-5606.0001889.

Conte, E. 2004. "Consolidation analysis for unsaturated soils." *Can. Geotech. J.* 41 (4): 599–612. https://doi.org/10.1139/t04-017.

Cozzolino, V. M. 1961. "Statistical forecasting of compression index." In Vol. 1 of *Proc., 5th Int. Conf. on Soil Mechanics and Foundation Engineering, Paris, France*, 51–53. Rotterdam, Netherlands: A.A. Balkema.

Deng, A., and Y. Zhou. 2015. "Modeling electroosmosis and surcharge preloading consolidation. I. Model formulation." *J. Geotech. Geoenviron. Eng.* 142 (4): 04015093. https://doi.org/10.1061/(ASCE)GT.1943-5606.0001417.

Dong, Y., and N. Lu. 2016a. "Correlation between small-strain shear modulus and suction stress in capillary regime under zero total stress conditions." *J. Geotech. Geoenviron. Eng.* 142 (11): 04016056. https://doi.org/10.1061/(ASCE)GT.1943-5606.0001531.

Dong, Y., and N. Lu. 2016b. "Dependencies of shear wave velocity and shear modulus of soil on saturation." *J. Eng. Mech.* 142 (11): 04016083. https://doi.org/10.1061/(ASCE)EM.1943-7889.0001147.

Dong, Y., and N. Lu. 2017. "Measurement of suction stress characteristic curve under drying and wetting conditions." *Geotech. Test. J.* 40 (1): 107–121. https://doi.org/10.1520/GTJ20160058.

Dong, Y., N. Lu, and J. S. McCartney. 2016. "A unified model for small-strain shear modulus of variably saturated soil." *J. Geotech. Geoenviron. Eng.* 142 (9): 04016039. https://doi.org/10.1061/(ASCE)GT.1943-5606.0001506.

Dong, Y., N. Lu, and J. S. McCartney. 2018. "Scaling shear modulus from small to finite strain for unsaturated soils." *J. Geotech. Geoenviron. Eng.* 144 (2): 04017110. https://doi.org/10.1061/(ASCE)GT.1943-5606.0001819.

Fleureau, J., S. Kheirbek-Saoud, R. Soemitro, and S. Taibi. 1993. "Behavior of clayey soils on drying-wetting paths." *Can. Geotech. J.* 30 (2): 287–296. https://doi.org/10.1139/t93-024.

Fleureau, J., J. Verbrugge, P. J. Huergo, A. G. Correia, and S. Kheirbek-Saoud. 2002. "Aspects of the behaviour of compacted clayey soils on drying and wetting paths." *Can. Geotech. J.* 39 (6): 1341–1357. https://doi.org/10.1139/t02-100.

Fox, P. J. 2000. "CS4: A large strain consolidation model for accreting soil layers." In *Geotechnics of high water content materials, STP 1374*, edited by T. B. Edil and P. J. Fox, 29–47. West Conshohocken, PA: ASTM.

Fox, P. J. 2007a. "Coupled large strain consolidation and solute transport. I. Model development." *J. Geotech. Geoenviron. Eng.* 133 (1): 3–15. https://doi.org/10.1061/(ASCE)1090-0241(2007)133:1(3).

Fox, P. J. 2007b. "Coupled large strain consolidation and solute transport. II. Model verification and simulation results." *J. Geotech. Geoenviron. Eng.* 133 (1): 16–29. https://doi.org/10.1061/(ASCE)1090-0241(2007)133:1(16).

Fox, P. J., and J. D. Berles. 1997. "CS2: A piecewise-linear model for large strain consolidation." *Int. J. Numer. Anal. Methods Geomech.* 21 (7): 453–475. https://doi.org/10.1002/(SICI)1096-9853(199707)21:7<453::AID-NAG887>3.0.CO;2-B.

Fox, P. J., M. Di Nicola, and D. W. Quigley. 2003. "Piecewise-linear model for large strain radial consolidation." *J. Geotech. Geoenviron. Eng.* 129 (10): 940–950. https://doi.org/10.1061/(ASCE)1090-0241(2003)129:10(940).

Fox, P. J., H. Pu, and J. D. Berles. 2014. "CS3: Large strain consolidation model for layered soils." *J. Geotech. Geoenviron. Eng.* 140 (8): 04014041. https://doi.org/10.1061/(ASCE)GT.1943-5606.0001128.

Fredlund, D. G., and J. U. Hasan. 1979. "One-dimensional consolidation theory: Unsaturated soils." *Can. Geotech. J.* 16 (3): 521–531. https://doi.org/10.1139/t79-058.

Gens, A., and E. E. Alonso. 1992. "A framework for the behaviour of unsaturated expansive clays." *Can. Geotech. J.* 29 (6): 1013–1032. https://doi.org/10.1139/t92-120.

Gibson, R. E., G. L. England, and M. J. L. Hussey. 1967. "The theory of one-dimensional consolidation of saturated clays. I: Finite non-linear consolidation of thin homogeneous layers." *Géotechnique* 17 (3): 261–273. https://doi.org/10.1680/geot.1967.17.3.261.

Gibson, R. E., R. L. Schiffman, and K. W. Cargill. 1981. "The theory of one-dimensional consolidation of saturated clays. II: Finite non-linear consolidation of thick homogeneous layers." *Can. Geotech. J.* 18 (2): 280–293. https://doi.org/10.1139/t81-030.

Indraratna, B., R. Zhong, P. Fox, and C. Rujikiatkamjorn. 2016. "Large-strain vacuum-assisted consolidation with non-Darcian radial flow incorporating varying permeability and compressibility." *J. Geotech. Geoenviron. Eng.* 143 (1): 04016088. https://doi.org/10.1061/(ASCE)GT.1943-5606.0001599.

Khalili, N., M. H. Khabbaz, and S. Valliappan. 2000. "An effective stress based numerical model for hydro-mechanical analysis in unsaturated porous media." *Comput. Mech.* 26 (2): 174–184. https://doi.org/10.1007/s004660000165.

Khorshidi, M., and N. Lu. 2016. "Intrinsic relationship between specific surface area and soil water retention." *J. Geotech. Geoenviron. Eng.* 143 (1): 04016078. https://doi.org/10.1061/(ASCE)GT.1943-5606.0001572.

Khorshidi, M., and N. Lu. 2017. "Determination of cation exchange capacity from soil water retention curve." *J. Eng. Mech.* 143 (6): 04017023. https://doi.org/10.1061/(ASCE)EM.1943-7889.0001220.

Krosley, L., W. Likos, and N. Lu. 2003. "Alternative encasement materials for Clod test." *Geotech. Test. J.* 26 (4): 461–463. https://doi.org/10.1520/GTJ11259J.

Likos, W. J., N. Lu, and W. Wenszel. 2011. "Performance of a dynamic dew point method for moisture isotherms of clays." *Geotech. Test. J.* 34 (4): 1–10. https://doi.org/10.1520/GTJ102901.

Lloret, A., and E. E. Alonso. 1980. "Consolidation of unsaturated soils including swelling and collapse behaviour." *Géotechnique* 30 (4): 449–477. https://doi.org/10.1680/geot.1980.30.4.449.

Lu, N. 2016. "Generalized soil water retention equation for adsorption and capillarity." *J. Geotech. Geoenviron. Eng.* 142 (10): 04016051. https://doi.org/10.1061/(ASCE)GT.1943-5606.0001524.

Lu, N., and Y. Dong. 2017a. "Correlation between soil shrinkage curve and water retention characteristics." *J. Geotech. Geoenviron. Eng.* 143 (9): 04017054. https://doi.org/10.1061/(ASCE)GT.1943-5606.0001741.

Lu, N., and Y. Dong. 2017b. "Vapor condensation technique for measuring stress-strain relation of unsaturated soil." *J. Geotech. Geoenviron. Eng.* 143 (6): 02817002. https://doi.org/10.1061/(ASCE)GT.1943-5606.0001656.

Lu, N., and Y. Dong. 2019. "Erratum for "Correlation between soil-shrinkage curve and water-retention characteristics" by Ning Lu and Yi Dong." *J. Geotech. Geoenviron. Eng.* 145 (8): 08219002. https://doi.org/10.1061/(ASCE)GT.1943-5606.0002090.

Lu, N., J. W. Godt, and D. T. Wu. 2010. "A closed-form equation for effective stress in unsaturated soil." *Water Resour. Res.* 46 (5): W05515. https://doi.org/10.1029/2009WR008646.
Lu, N., and M. Kaya. 2013. "A drying cake method for measuring suction-stress characteristic curve, soil-water-retention curve, and hydraulic conductivity function." *Geotech. Test. J.* 36 (1): 20120097. https://doi.org/10.1520/GTJ20120097.
Lu, N., and M. Kaya. 2014. "Power law for elastic moduli of unsaturated soil." *J. Geotech. Geoenviron. Eng.* 140 (1): 46–56. https://doi.org/10.1061/(ASCE)GT.1943-5606.0000990.
Lu, N., and M. Khorshidi. 2015. "Mechanism for soil-water retention and hysteresis at high suction range." *J. Geotech. Geoenviron. Eng.* 141 (8): 04015032. https://doi.org/10.1061/(ASCE)GT.1943-5606.0001325.
Lu, N., T. H. Kim, S. Sture, and W. J. Likos. 2009. "Tensile strength of unsaturated sand." *J. Eng. Mech.* 135 (12): 1410–1419. https://doi.org/10.1061/(ASCE)EM.1943-7889.0000054.
Lu, N., and W. J. Likos. 2004. *Unsaturated soil mechanics*. New York: Wiley.
Lu, N., and W. J. Likos. 2006. "Suction stress characteristic curve for unsaturated soils." *J. Geotech. Geoenviron. Eng.* 132 (2): 131–142. https://doi.org/10.1061/(ASCE)1090-0241(2006)132:2(131).
Mayne, P. W. 1980. "Cam-clay predictions of undrained strength." *J. Geotech. Eng. Div.* 106(11): 1219–1242.
McKeen, R. G. 1992. "A model for predicting expansive soil behavior." In *Proc., 7th Int. Conf. on Expansive Soils*, 1–6. Reston, VA: ASCE.
Mun, W., and J. S. McCartney. 2015. "Compression mechanisms of unsaturated clay under high stresses." *Can. Geotech. J.* 52 (12): 2099–2112. https://doi.org/10.1139/cgj-2014-0438.
Pu, H., P. J. Fox, and Y. Liu. 2013. "Model for large strain consolidation under constant rate of strain." *Int. J. Numer. Anal. Methods Geomech.* 37 (11): 1574–1590. https://doi.org/10.1002/nag.2100.
Santamarina, J. C., K. A. Klein, and M. A. Fam. 2001. *Soils and waves*. New York: Wiley.
Schrefler, B. A., and X. Y. Zhan. 1993. "A fully coupled model for water flow and airflow in deformable porous media." *Water Resour. Res.* 29 (1): 155–167. https://doi.org/10.1029/92WR01737.
Sharkey, K. 2002. "Geotechnical engineering behavior of Denver expansive clay shale." M.S. thesis, Dept. of Civil and Environmental Engineering, Colorado School of Mines.
Sheng, D. C., D. G. Fredlund, and A. Gens. 2008. "A new modelling approach for unsaturated soils using independent stress variables." *Geotech. Test. J.* 45 (4): 511–534. https://doi.org/10.1139/T07-112.
Skempton, A. W. 1944. "Notes on the compressibility of clays." *Q. J. Geol. Soc. London* 100 (1–4): 119–135. https://doi.org/10.1144/GSL.JGS.1944.100.01-04.08.
Terzaghi, K. 1943. *Theoretical soil mechanics*. New York: Wiley.
Terzaghi, K., and R. B. Peck. 1967. *Soil mechanics in engineering practice*. 2nd ed. New York: Wiley.
van Genuchten, M. T. 1980. "A closed-form equation for predicting the hydraulic conductivity of unsaturated soils." *Soil Sci. Soc. Am. J.* 44 (5): 892–898. https://doi.org/10.2136/sssaj1980.03615995004400050002x.
Wayllace, A., and N. Lu. 2012. "Transient water release and imbibitions method for rapidly measuring wetting and drying soil water retention and hydraulic conductivity functions." *Geotech. Test. J.* 35 (1): 1–15. https://doi.org/10.1520/GTJ103596.
Wei, C. 2014. "A theoretical framework for modeling the chemomechanical behavior of unsaturated soils." *Vadose Zone J.* 13 (9): 1–21. https://doi.org/10.2136/vzj2013.07.0132.
Wheeler, S. J., R. S. Sharma, and M. S. R. Buisson. 2003. "Coupling of hydraulic hysteresis and stress–strain behaviour in unsaturated soils." *Géotechnique* 53 (1): 41–54. https://doi.org/10.1680/geot.2003.53.1.41.
White, D. J., W. A. Take, and M. D. Bolton. 2003. "Soil deformation measurement using particle image velocimetry (PIV) and photogrammetry." *Géotechnique* 53 (7): 619–631. https://doi.org/10.1680/geot.2003.53.7.619.
Wissa, A. E. Z., J. T. Christian, E. H. Davis, and S. Heiberg. 1971. "Consolidation at constant rate of strain." *J. Soil Mech. Found. Div.* 97 (10): 1393–1413.
Wood, D. M. 1990. *Soil behaviour and critical state soil mechanics*. Cambridge, UK: Cambridge University Press.
Zhou, A. N., D. C. Sheng, S. W. Sloan, and A. Gens. 2012. "Interpretation of unsaturated soil behaviour in the stress–saturation space II: Constitutive relationships and validations." *Comput. Geotech.* 43 (Jun): 111–123. https://doi.org/10.1016/j.compgeo.2012.02.009.